Published in final edited form as:
Neuron. 2013 June 19; 78(6): 1012–1023. doi:10.1016/j.neuron.2013.05.010.

mSYD1A, a Mammalian Synapse-Defective-1 Protein, Regulates Synaptogenic Signaling and Vesicle Docking

Corinna Wentzel[1], **Julia Sommer**[1,*], **Ramya Nair**[1,*], **Adeline Stiefvater**[1], **Jean-Baptiste Sibarita**[2,3], and **Peter Scheiffele**[1]

[1]Biozentrum, University of Basel, 4056 Basel, Switzerland [2]University of Bordeaux, Interdisciplinary Institute for Neuroscience, Bordeaux, France [3]CNRS UMR 5297, F-33000 Bordeaux, France

Summary

Structure and function of presynaptic terminals are critical for the transmission and processing of neuronal signals. Trans-synaptic signaling systems instruct the differentiation and function of presynaptic release sites but their downstream mediators are only beginning to be understood. Here, we identify the intracellular mSYD1A (mouse Synapse-Defective-1A) as a novel regulator of presynaptic function in mice. mSYD1A forms a complex with presynaptic receptor tyrosine phosphatases and controls tethering of synaptic vesicles at synapses. mSYD1A function relies on an intrinsically disordered domain that interacts with multiple structurally-unrelated binding partners, including the active zone protein liprin-α2 and nsec1/munc18-1. In mSYD1A knock-out mice, synapses assemble in normal numbers but there is a significant reduction in synaptic vesicle docking at the active zone and an impairment of synaptic transmission. Thus, mSYD1A is a novel regulator of presynaptic release sites at central synapses.

Introduction

The differentiation of synaptic terminals encompasses a profound re-organization of the axonal cytoskeleton and presynaptic membrane organelles. Hallmarks of this morphogenetic process are the assembly of active zones, accumulation of synaptic vesicles in the terminal, and the docking of a pool of vesicles at the release sites. At mature synapses, a complex cytoplasmic network consisting of scaffolding and cytomatrix proteins orchestrates morphological and functional properties of release sites (Zhai and Bellen, 2004; Ziv and Garner, 2004; Arikkath and Reichardt, 2008; Shen and Scheiffele, 2010; Gundelfinger and Fejtova, 2012; Südhof, 2012). The large ELKS, piccolo, and bassoon proteins represent major structural building blocks of the cytomatrix. Moreover, munc18, munc13, RIM and CAPS proteins are essential for the maintenance of a docked pool of synaptic vesicles (Weimer et al., 2003; Jockusch et al., 2007; Verhage and Sorensen, 2008; Siksou et al., 2009; Han et al., 2011). Several trans-synaptic signaling systems have been implicated in instructing the presynaptic differentiation process but the cytoplasmic mechanisms that relay

Correspondence: Peter Scheiffele, Biozentrum, University of Basel, Klingelbergstrasse 50-70, 4056 Basel, Switzerland, peter.scheiffele@unibas.ch.

*both authors made similar contributions to this work

such signals are only beginning to emerge (Biederer and Stagi, 2008; Johnson et al., 2009). In mammals, a Fer/Beta-catenin/beta-PIX signaling cascade modulates the overall abundance of synaptic vesicles in presynaptic terminals through organization of the actin cytoskeleton (Sun and Bamji, 2011). However, molecular mechanisms that link cell surface receptors to cytoplasmic regulators of active zone morphogenesis, synaptic vesicle accumulation and docking remain to be identified.

Many key regulators of synaptic vesicle recruitment have been discovered in powerful forward genetic screens in invertebrates (Jin and Garner, 2008; Johnson et al., 2009; Miskiewicz et al., 2011; Sigrist and Schmitz, 2011; Stavoe and Colon-Ramos, 2012). Amongst these is synapse-defective-1, a cytosolic protein implicated in presynaptic differentiation. In *C.elegans syd-1* mutants, active zone components and synaptic vesicles are dispersed along neuronal processes (Hallam et al., 2002). Genetic experiments demonstrate that SYD-1 acts downstream of surface receptors SYG-1 and PTP-3 (a receptor tyrosine phosphatase) and upstream of the active zone proteins SYD-2, ELKS-1 and MIG-10/lamellopodin (Ackley et al., 2005; Dai et al., 2006; Patel et al., 2006; Biederer and Stagi, 2008; Stavoe and Colon-Ramos, 2012). SYD-1 functions might be mediated through a Rho-GAP-like domain of the protein and a PDZ domain that links SYD-1 to the surface receptor neurexin (Hallam et al., 2002; Owald et al., 2012). Notably, mammalian genomes do not appear to encode proteins that precisely match the domain organization of invertebrate *syd-1* and to date no mammalian orthologues of SYD-1 have been characterized.

Here, we identify a mouse SYD-1 orthologue (mSYD1A) that regulates presynaptic differentiation. Surprisingly, mSYD1A function depends on a previously undescribed intrinsically disordered domain. This domain represents a unique multifunctional interaction module that associates with several presynaptic proteins, including nsec1/munc18-1, a key regulator of synaptic transmission. Synapses in mSYD1A knock-out hippocampus exhibit a severe reduction in morphologically docked vesicles and reduced synaptic transmission. These findings uncover mSYD1A as a novel regulator of synaptic vesicle docking in the presynaptic terminal.

Results

mSYD1A is expressed during the time of synapse formation and associates with synaptic membranes

Based on sequence similarity we considered *syde1*/NP_082151.1 (in the following referred to as *msyd1a*) and *syde2*/NP_001159536 (*msyd1b*) as the most plausible candidate orthologues (Figure S1A). The mSYD1 proteins share C2 and Rho-GAP domains but lack the N-terminal PDZ-domain sequences observed in the invertebrate proteins (Figure 1A). HA-epitope tagged mSYD1A and mSYD1B proteins have an apparent molecular weight of 100 and 150 kDa, respectively (Figure 1B, “cDNA”). An affinity-purified antibody raised against the N-terminus of mSYD1A recognized overexpressed mSYD1A but not mSYD1B. Expression of endogenous mSYD1A was observed in lysates of purified cerebellar granule cells (GC), mouse brain extracts and HEK293 cells (Figure 1B,C, see Figure S1C for expression during development) and specificity of antibody detection was confirmed by RNA interference knockdown (Figure 1C).

A remarkable feature of mammalian SYD1 proteins is the presence of extensive stretches of N-terminal sequences that are predicted to be intrinsically disordered (Figure 1D, S1B). Intrinsic disorder has been hypothesized to endow proteins with an ability to adapt to multiple specific binding partners and to contribute to the assembly of macromolecular arrays (Dyson and Wright, 2005; Tompa, 2012). We performed heat-denaturation

experiments to test experimentally whether the N-terminal domain of mSYD1A is indeed intrinsically disordered. Globular proteins denature and precipitate after prolonged heat exposure whereas intrinsically disordered domains exhibit heat stability (Hackel et al., 2000; Galea et al., 2006). Full-length mSYD1A and the GAP domain were rendered insoluble after heating cell extracts to 90°C for 30 min or 1 hour. By contrast, the mSYD1A N-terminal domain was resistant to thermal denaturation (Figure 1E). Thus, mSYD1A contains an intrinsically disordered domain (IDD) at the N-terminus.

To address whether mSYD1A is found at synapses, we isolated synaptosomal membranes from adult mouse brain (Figure 1F). mSYD1A was recovered in brain cytosol (S2) but also in the crude purified synaptosomal fractions (P2). After lysis of the synaptosomes, similar amounts of mSYD1A were associated with the Triton X-100 soluble and insoluble fractions. Finally, we examined the localization of epitope-tagged mSYD1A that was overexpressed in cultured cerebellar granule neurons. Within axons immune-reactivity was observed in a punctate pattern with a significant fraction of mSYD1A accumulations also containing synaptic markers vGluT1 and PSD95 (Figure 1G). In combination, these findings demonstrate that mSYD1A is expressed in the developing brain with pools of the protein associated with synaptic structures.

mSYD1A is required for presynaptic assembly

We probed a requirement for mSYD1A in presynaptic differentiation using RNA interference. Small double-stranded RNAs were applied conjugated to a cell membrane penetrating tag, which allows for efficient mSYD1A knockdown in the majority of cells (Figure S2A). To measure the density of synaptic terminals in axons we marked synaptic vesicles in a subset of cells by transfection of a synaptophysin-mCherry fusion protein (Figure 2A, note that synaptophysin-mCherry expression did not significantly alter distribution of endogenous vGluT1, Figure S2H). Postsynaptic elements were visualized by immunostaining for PSD95. Morphometric analysis of synaptic markers was performed by a wavelet-based segmentation method with a Multidimensional Image Analysis (MIA) module (Racine et al., 2006; Izeddin et al., 2012) that enables reliable quantitative assessment of synaptic markers. In mSYD1A knockdown neurons, the mean density of synaptophysin-mCherry-positive puncta was reduced by 39 ± 8 % whereas the density of PSD95-containing structures was not significantly altered (Figure 2B–D). Furthermore, the intensities of synaptophysin-mCherry-positive puncta were reduced in mSYD1A knockdown neurons, with puncta of higher intensities being less frequent ($p<0.002$, Figure 2E). Reduction in the accumulation of synaptic vesicles was also observed using the marker vGluT1 in absence of any exogenous vesicle protein expression (Figure S2G). The active zone protein munc13-1 was not noticeably altered whereas the density of detectable bassoon-positive clusters was slightly reduced in mSYD1A knockdown neurons (Figure 2F). Notably, the density of structures double positive for either presynaptic active zone markers and postsynaptic scaffolding proteins (homer, PSD95) was unaltered, indicating that mSYD1A loss in cultured neurons does not change synapse density but only presynaptic composition (Figure 2F). We tested whether function of mSYD1A is specifically required in the presynaptic cell by introducing a human, siRNA-resistant form of SYD1A (hSYD1A) into the synaptophysin-mCherry-positive cells. Importantly, this was sufficient to rescue the presynaptic terminal and synapse density back to wild-type level (Figure 2C,D).

Recording of miniature excitatory postsynaptic currents (mEPSCs) in mSYD1A knockdown cultures further supported a presynaptic phenotype. The mEPSC frequency in knockdown neurons was reduced by 43 ± 7% as compared to controls (Figure 2G). This reduction was rescued by re-introduction of hSYD1A using lenti-viral infection (see Figure S2 for re-expression level and further controls for the RNA interference experiments). In combination with the morphological effects on synaptic vesicle distribution these results demonstrate that

mSYD1A controls presynaptic differentiation in cultured neurons and is required in the presynaptic cell.

mSYD1A exhibits GAP activity towards RhoA

Some functions of invertebrate SYD-1 proteins are thought to rely on a catalytically inactive Rho-GAP-like domain whereas others have been pinpointed to the PDZ-domain of the protein (Hallam et al., 2002; Owald et al., 2012). Mammalian SYD1 proteins differ significantly from their invertebrate counterparts in that they lack PDZ-domains and contain Rho-GAP domains that may be active based on amino acid sequence analysis (Figure S3A). We directly probed GAP activity of mSYD1A in intact cells using a FRET-based assay (Itoh et al., 2002; Pertz et al., 2006) (Figure 3A). Using a RhoA sensor, we observed significant RhoA inactivation in cells expressing mSYD1A. The degree of RhoA inactivation was similar to that observed for p50rhoGAP, a well-characterized GAP (Figure 3B,C). Importantly, mutation of the arginine finger (Graham et al., 1999) in mSYD1A (R436A) strongly reduced mSYD1A activity observed in this assay and no change in FRET was observed when Lin-2/CASK, a protein lacking GAP domains, was introduced (Figure 3B,C). Similarly, the amino acid alterations from the Rho-GAP consensus seen in the *C.elegans* and *Drosophila* SYD-1 proteins strongly reduce activity towards RhoA (Figure S3B). Finally, we used morphological changes of neuronal dendrites as a read-out for RhoA regulation in cerebellar granule cells. Over-expression of C-terminally Myc-tagged mSYD1A but not the R436A or ΔYRL mutants led to a significant increase in dendritic trees compared to GFP-transfected neurons (Figure S3D). These morphological readouts are consistent with an inactivation of endogenous RhoA-dependent contractility by mSYD1A. Therefore, mSYD1A is a functional Rho-GAP whereas amino acid substitutions present in the invertebrate SYD-1 proteins render the GAP domain inactive.

Interestingly, the mammalian SYD1A GAP activity is regulated through intramolecular interactions. Deletion of the intrinsically disordered domain (IDD) and C2 domain resulted in a doubling of mSYD1A GAP activity (Figure 3D–F). A similar increase was observed when full-length mSYD1A was targeted to the plasma membrane with an N-terminal lipid modification (myr-mSYD1A) suggesting that full-length mSYD1A is in an auto-inhibitory conformation and can be activated by the displacement of N-terminal sequences (Figure 3E). When we co-expressed IDD and GAP domains as independent polypeptides (Figure 3G), the IDD alone as well as the IDD-C2 domain supplied in *cis* where able to repress activity of the isolated mSYD1A GAP domain. Finally, we tested whether the inhibition of mSYD1A GAP activity is mediated through protein-protein interactions between the IDD and GAP domains in co-immunoprecipitation experiments (Figure 3H). Myc-tagged GAP domain was co-immunoprecipitated with the HA-tagged IDD-C2 domain. Thus, the mSYD1A GAP activity is regulated through protein-protein interactions with the intrinsically disordered N-terminal domain suggesting that full-length mSYD1A adopts a closed, auto-inhibited conformation. Displacement of the IDD, either by truncation or membrane targeting, provides a mechanism for local activation of mSYD1A.

Synaptogenic function of mSYD1A relies on the intrinsically disordered domain

We tested the functional relevance of the mSYD1A subdomains in synapse formation using gain-of-function experiments. Overexpression of full-length mSYD1A in cultured granule cells resulted in a 64 ± 10 % elevation in the density of synaptic vesicle clusters and a 38 ± 11 % increase in synapse density, defined as puncta containing the markers synaptophysin and PSD95. Thus, presynaptic over-expression of mSYD1A is sufficient to stimulate pre- and postsynaptic differentiation. Surprisingly, a mSYD1A mutant lacking the arginine finger (ΔYRL) lost the ability to recruit the postsynaptic marker PSD95 but retained the ability to elevate presynaptic terminal number (Figure 4B). Moreover, a membrane-targeted form of

the IDD (that lacks the entire C2 and GAP domain sequences of mSYD1A) was sufficient to increase presynaptic terminal density and partially co-localized with the synaptic vesicle marker vGluT1 in axons (Figure 4A,B). Importantly, this function of the IDD was also observed when the protein was expressed in neurons lacking full-length mSYD1A expression ruling out an indirect effect through modification of the endogenous protein (Figure S4A). Thus, the IDD is sufficient to drive recruitment of synaptic vesicles independently of the mSYD1A GAP activity.

Given the critical importance of the IDD for mSYD1A function we performed a yeast two-hybrid screen with this domain as a bait to identify binding partners. We isolated an N-terminal fragment of nsec1/munc18-1 as a candidate interaction partner (Figure 4C). mSYD1A – munc18-1 interactions were confirmed in coimmunoprecipitation experiments were munc18-1 was recovered in immunoprecipitates with full-length mSYD1A (Figure 4D). In pull-down experiments with recombinant munc18-1 coupled to beads, constructs containing the IDD and the IDD-C2 domain of mSYD1A bound to munc18-1, but not the GAP domain (Figure 4E). Thus, mSYD1A binds to munc18-1, a key component of the vesicle docking and fusion machinery. Genetic experiments in *C.elegans* identified SYD-2/liprin as acting in the same pathway as SYD-1 (Hallam et al., 2002). However, no physical interactions between SYD-1/SYD-2 proteins have been reported. We tested whether mammalian liprin-α might represent an additional mSYD1A interaction partner. In pull-down assays with purified recombinant fragments of liprin-α proteins, we identified the SAM-domains located in the C-terminal half of liprin-α2 as interaction site (Figure 4F,H) whereas no binding was observed to the coiled-coil domains of liprin-α (Figure 4G, functionality of the recombinant proteins confirmed by interaction with ELKS2 (Ko et al., 2003)). Surprisingly, the interaction with mSYD1A was strictly liprin-α isoform-specific. The mammalian liprin-α2 protein contains a 37 amino acid insertion located between the first and the second SAM domain that is absent in the primary liprin-α1 isoform and invertebrate liprin/SYD-2 proteins (Zürner and Schoch, 2009; Wei et al., 2011) (Figure 4H). Deletion of these 37 amino acids (SAMΔPQ) abolished binding between mSYD1A and liprin-α2 (Figure 4F, see Figure S4B for recombinant proteins). Binding efficiency of mSYD1A was comparable to Lin-2/CASK, a previously characterized liprin-α2 interactor whereas no binding to X11α/ Mint1 was detected. Importantly, we mapped the interaction domain within mSYD1A to the IDD (Figure S4C) and confirmed a direct protein-protein interaction between purified recombinant liprin-α2-SAM and purified mSYD1A IDD (Figure 4I). Thus, the N-terminal intrinsically disordered domain of mSYD1A is a critical functional module that binds at least three different ligands: the mSYD1A GAP domain, nsec1/munc18-1, and liprin-α2.

LAR/liprin-α2/ mSYD1A complex

The biochemical interactions between mSYD1A and the active zone protein liprin-α2 raise the question whether mSYD1A and liprin-α2 act in a complex downstream of receptor protein tyrosine phosphatases that recruit liprins and contribute to synapse formation (Kwon et al., 2010; Takahashi et al., 2011; Yoshida et al., 2011). In COS7 cells, we observed the formation of macroscopic complexes that concentrate LAR, liprin-α2, and mSYD1A (Figure 5A, S5A–C). Deletion of the mSYD1A IDD abolished its recruitment to these structures (Figure 5A,B) (Pearson's coefficient, 0.85 ± 0.05). We further explored the formation of mSYD1A/liprin-α2/LAR complexes in coimmunoprecipitation assays. Antibodies to mSYD1A co-precipitated liprin-α2 and LAR proteins, therefore, linking these proteins in a signaling complex (Figure 5C). We then explored whether mSYD1A functionally contributes to presynaptic assembly downstream of LAR. We stimulated presynaptic differentiation in cultured neurons by overexpression of NGL-3, a postsynaptic interaction partner for presynaptic LAR (Woo et al., 2009). Overexpression of NGL-3 led to

a significant elevation in the density of vGluT1 and bassoon puncta along the dendrites of transfected neurons (Figure 5D,E). Knockdown of mSYD1A significantly attenuated this increase (Figure 5D,E; note that surface expression level of NGL-3 was unchanged, Figure S5D). We observed a similar inhibition of presynaptic differentiation by mSYD1A knock-down on GFP control neurons and neurons overexpressing the synaptogenic adhesion molecule neuroligin-1. Thus, the requirement of mSYD1A in presynaptic differentiation is not unique to the NGL-3/LAR receptor system but most likely common to multiple presynaptic signalling pathways.

Loss of docked vesicles and impaired synaptic transmission in *mSYD1A^{KO}* hippocampus

To probe the function of mSYD1A in intact neuronal circuits *in vivo* we generated mSYD1A mutant mice (*mSYD1A^{KO}*). Mutant mice were generated by blastocyst injection of targeted ES cells carrying a genetrap insertion between the first and second exon (Figure 6A) (Skarnes et al., 2011). In homozygous mutant mice immune-reactivity for the mSYD1A protein was abolished (Figure 6B). Homozygous mutant animals are born at Mendelian frequencies, are viable, fertile and show indistinguishable weight gain during the first four weeks of life (Figure 6C,D). Gross brain anatomy was not noticeably altered (Figure 6E and data not shown). Given that hippocampal synapses are particularly accessible for functional analysis, we examined synaptic transmission in CA1 pyramidal cells of acute hippocampal slices. The frequency of mEPSCs was significantly reduced (Figure 6F). By contrast, mEPSC amplitudes were unchanged. Paired-pulse ratios were indistinguishable between wild-type and *mSYD1A^{KO}* cells suggesting that the probability of release was unaltered (Figure 6G).

The reduction in mEPSC frequency could result from either a loss of synapses or a disruption of presynaptic function. We explored the density and ultrastructure of synapses in the mSYD1A knock-out by quantitative ultrastructural analyses of synapses in the *stratum radiatum* of hippocampal area CA1. We observed no significant alterations in the density and size of asymmetric synapses, arguing against a change in glutamatergic synapse number ($p=0.47$, 147 and 157 9.3 μm^2 fields, from four wild-type and four knock-out animals, respectively, Figure 7A,B). Therefore, we further explored the distribution of synaptic vesicles in synaptic terminals, in particular, the docking of vesicles at active zones. This analysis revealed a striking reduction in morphologically docked vesicles at *mSYD1A^{KO}* synapses in CA1 (Figure 7C,D). Cumulative probability plots of the vesicle distribution close to the active zone (within 50 nm) show a significant shift of this vesicle population away from the active zone ($p<0.001$, Figure 7E). Similarly, an analysis of the vesicle density across bins of increasing distance from the active zone confirms a selective reduction in vesicle density within the first 80 nm of the active zone but no significant change in the more distant populations of vesicles (Figure 7F). Therefore, mSYD1A is essential for maintaining morphologically docked vesicles at the active zone *in vivo*.

Discussion

In this study we report a novel regulator of synaptic differentiation that is essential for synaptic vesicle docking at central synapses. We initially identified mSYD1A based on sequence similarity with the invertebrate SYD-1 proteins. However, mSYD1A should be considered a distant orthologue for several reasons. First, mammalian and invertebrate SYD1s share significant sequence homology only in their C2 and GAP domains. Second, the PDZ domain, a key element of invertebrate SYD-1 (Owald et al., 2012), is absent from the vertebrate counterparts. Third, the invertebrate Rho-GAP domains are catalytically inactive whereas mSYD1A does exhibit GAP activity, which contributes to trans-synaptic signaling (at least in over-expression experiments, Figure 4). Fourth, a unique intrinsically disordered (ID) domain in mSYD1A is a key element for mSYD1A function. Liprin-α2

binding to the ID-domain requires a specific insertion in liprin-α2 (PQ-loop) that is lacking in liprin-α1. Given that liprin-α1 and α2 isoforms are differentially expressed throughout the brain (Spangler et al., 2011; Zürner et al., 2011) this might result in synapse-specific liprin-mSYD1A coupling. Notably, this insertion is not present in the invertebrate SYD-2s, highlighting the possibility that this direct biochemical interaction is unique for vertebrates. Thus, in mammalian SYD1 proteins certain divergent mechanisms of function have evolved.

An intrinsically disordered domain as presynaptic regulator

Multiple Rho-GTPase regulators (GAPs and GEFs) have been previously recognized as regulators of synapse size and tethering of synaptic vesicles at presynaptic release sites (Frank et al., 2009; Ball et al., 2010; Sun and Bamji, 2011; Cheadle and Biederer, 2012). Surprisingly, the ability of mSYD1A to stimulate presynaptic differentiation in cultured neurons does not require its GAP activity but relies on its ID-domain. Intrinsically disordered proteins are starting to be recognized as critical mediators of multiple biological processes, including assembly of protein-RNA granules, transcriptional activation, and nonsense-mediated decay (Tompa, 2012). ID-domains have the ability to undergo transitions from disordered to ordered conformations upon contact with specific binding partners or in response to post-translational modification. These properties enable ID-domains to engage with multiple, structurally diverse effectors. The mSYD1A ID-domain provides a remarkable example for this molecular multi-tasking as it couples to three structurally unrelated binding partners: nsec1/munc18-1, the liprin-α2 SAM-domains, and the mSYD1A GAP domain. Previous studies on presynaptic protein function have largely focused on structured domains and their potential for scaffolding interactions. We surveyed eleven major synaptic proteins and observed that several of them contain extended stretches (>200 amino acids) of continuous intrinsically disordered sequence (caskin1, ELKS1, munc13-1, piccolo, RIM1, but not GRIP1, Lin-2/CASK, munc18-1, PSD95, syntenin-1, X11α/mint1, data not shown). We propose that intrinsically disordered protein domains might be more broadly used to control presynaptic assembly and function. Their properties are ideally suited as they accommodate a multitude of finely tuned protein-protein interactions and their dynamic regulation by post-translational modifications (Tompa, 2012).

Essential function of mSYD1A in synaptic vesicle docking

Work on the invertebrate SYD-1 mutants highlighted mis-localization of synaptic vesicles and active zone components (Hallam et al., 2002; Owald et al., 2010). Our observations are consistent with an analogous function for mSYD1A in vesicle tethering at mammalian synapses in cultured neurons. However, in $mSYD1A^{KO}$ mice *in vivo* we did not observe a similarly severe dispersion of synaptic vesicles but instead uncovered a selective reduction in the docked vesicle pool. More subtle alterations in the total synaptic vesicle pool may have been undetectable in our analysis but, clearly, the reduction in docked vesicles is more severe than any potential reduction in the total vesicle pool. Thus, the depletion of the docked pool cannot be explained by an overall reduction in synaptic vesicles at these synapses (Marra et al., 2012). Expression of mSYD1B, the second mammalian SYD1 isoform, may partially compensate for the loss of mSYD1A and may attenuate effects on overall synaptic vesicle accumulation in $mSYD1A^{KO}$ synapses. Regardless, the reduction in vesicle docking in *mSYD1A* single KO mice is severe and, thus, reveals a novel function for a SYD1 protein *in vivo*. In cultured neurons, the mSYD1A IDD is sufficient to promote synaptic vesicle clustering but it remains to be explored whether the IDD is sufficient to rescue the synaptic vesicle docking phenotype in $mSYD1A^{KO}$ hippocampus. The docked vesicle pool is strongly correlated to the number of highly fusion competent vesicles at synapses (Schikorski and Stevens, 2001; Toonen et al., 2006; Han et al., 2011). Thus, a reduction in the docked pool is consistent with the significant reduction in spontaneous fusion events observed upon mSYD1A loss-of-function in vitro and in vivo. Notably, we

identified nsec1/munc18-1, a key factor implicated in vesicle docking (Weimer et al., 2003; Toonen et al., 2006), as binding partner of mSYD1A. Thus, mSYD1A provides a link between synaptogenic cell surface receptors such as LAR and the vesicle docking machinery of the presynaptic terminal.

Experimental Procedures—*Please see* Supplemental Experimental Procedures *for further details*

Antibodies—Rabbit polyclonal antibodies against mSYD1A were raised against a synthetic peptide (MAEPLLRKTFSRLRGREK) and affinity purified on the antigen. Anti-pan-neuroligin was described previously (Taniguchi et al., 2007). Rabbit anti-munc18 was a gift from Matthijs Verhage (de Vries et al., 2000). Other antibodies were purchased from commercial sources: mouse anti-actin (clone AC-40, Sigma-Aldrich), goat anti-cyclinA (#sc-31086, Santa-Cruz), mouse anti-PSD95 (#73-028, Neuromab), mouse anti-VAMP2 (clone 69.1, Synaptic Systems), anti-vesicular glutamate transporter 1 (vGluT1, #1353303, Synaptic Systems), rabbit anti-GAPDH (#E1C604, Enogene), mouse anti-CASK (#75-000, Neuromab), rabbit anti-munc13-1 (#126103, Synaptic Systems), rabbit anti-munc18-1 (#116002, Synaptic Systems), mouse anti-beta-tubulin (E7, DSHB), rabbit anti-ELKS 1b/2 (#143003, Synaptic Systems), rat anti-HA (clone 3F10, Roche Applied Science), rabbit anti-c-myc (#sc-789, Santa-Cruz), mouse anti-flag (#F1804, Sigma), rabbit anti-homer (#160003, Synaptic Systems), mouse anti-bassoon (#GTX13249, GeneTex), rabbit anti-calbindin (#CB38a, Swant), mouse anti-NeuN (#MAB377, Chemicon). Secondary antibodies conjugated to cyanine dyes or Alexa 488 or 643 (Jackson ImmunoResearch and Invitrogen) were used for visualization in immunostainings.

Disorder Prediction and Thermostability Test—Candidate intrinsically disordered protein domains were predicted using the PrDOS server, an online tool that combines local amino acid information and template protein references (http://prdos.hgc.jp/cgi-bin/top.cgi) (Ishida and Kinoshita, 2008). The thermostability test for confirmation of intrinsically disordered sequences was performed as described previously (Galea et al., 2006). Briefly, HEK293T cells on 10 cm diameter dishes were transfected with expression constructs for mSYD1A. After 24 h, cells were harvested in PBS with a cell scraper and resuspended in 300 µl of Buffer A [10 mM sodium phosphate buffer, pH 7.0, 50 mM NaCl, 50 mM DTT, 0.1 mM sodium orthovanadate, complete protease inhibitor (Roche)]. Cells were mechanically cracked by passing through a 25G needle and centrifuged at 16,000 × g for 30 min at 4 °C . The supernatant was transferred to a fresh tu be and the protein concentration was adjusted to 1 mg/ml with Buffer A. The cell lysate was heated for 30 min or 1 h at 90 °C . The protein mixture was placed on ice for 15 min and centrifuged at 16,000 × g for 30 min at RT. Soluble proteins in the supernatant were precipitated with 10% trichloracetic acid. The pellets were resuspended in SDS-PAGE buffer and analyzed by western blotting.

Rho-GAP Assays—Förster-resonance energy transfer (FRET) assays were performed as described previously (Itoh et al., 2002). Briefly, HEK293T cells were transfected with the RhoA sensor (Pertz et al., 2006) and expression constructs of interest. After 48 h cells were suspended in 1x PBS. The emission spectrum between 450–600 nm after excitation with 430 nm light was measured in a Fluorescence Spectrophotometer (FP-6500, Jasco). Following the measurement cells were lysed for protein expression analysis.

Cellular Assays—For co-aggregation experiments COS7 cells were transiently transfected (Fugene, Roche) and proteins were expressed for 48 h. Cells were fixed with 4 % PFA, 4 % sucrose in 100 mM sodium phosphate buffer (pH 7.4) for 15 min at room temperature. Immunostaining was done using standard procedures.

Dissociated cultures of mouse cerebellar granule cells were prepared from P5-P7 pups as described previously (Dean et al., 2003). Knockdown of *msyd-1a* was performed on day 1 (replenished at day 4) with 0.75 μM Accell SMART pool siRNA against *msyd-1a* or a non-target control pool (Dharmacon). At day 7, cells were fixed with 4 % paraformaldehyde, containing 4 % sucrose in 100 mM phosphate buffer (pH 7.4). After antibody staining the coverslips were mounted with ProLong (Invitrogen).

For lentiviral delivery of hSYD1A, a lentiviral vector with a dual human synapsin promoter was used to express GFP and hSYD1A (Gascon et al., 2008).

Electrophysiology—Whole cell patch clamp recordings were performed on DIV 8–11 cerebellar granule cell cultures. For rescue, the lentivirus was added at DIV 3. The extracellular solution (pH 7.3) contained the following: 145 mM NaCl, 5 mM KCl, 2 mM $CaCl_2$, 1 mM $MgCl_2$, 5 mM Glucose, 25 mM Sucrose and 5 mM HEPES. For all the experiments 300 nM TTX, 0.1 mM Picrotoxin and 0.1 mM AP5 were used in the solution. The internal solution contained the following: 130 mM CsCl, 10 mM HEPES, 10 mM EGTA, 10 mM Phosphocreatine, 2 mM MgATP, 5 mM NaCl, pH 7.25 and 298 mOsm.

For acute slice recordings, P11–16 mice were anesthetized with isoflurane and rapidly decapitated. 300 μm thick sagittal sections were cut in sucrose substituted artificial cerebrospinal fluid (ACSF) that consisted of: 83 mM NaCl, 2.5 mM KCl, 1 mM NaH_2PO_4, 26.2 mM $NaHCO_3$, 22 mM glucose, 72 mM sucrose, 0.5 mM $CaCl_2$, 3.3 mM $MgCl_2$. Slices were allowed to recover at 32 °C for 1 h a nd then maintained at room temperature in the same sucrose ACSF. For whole cell recordings, slices were perfused with: 119 mM NaCl, 2.5 mM KCl, 1 mM NaH_2PO_4, 26 mM $NaHCO_3$, 2 mM $CaCl_2$, 1.3 mM $MgSO_4$, 11 mM glucose, 0.1 mM Picrotoxin. For all experiments, whole cell recordings were digitized at 10 kHz and filtered at 2 kHz. Whole cell patch clamp recordings of CA1 pyramidal cells were done using 3–6M Ω pipettes and filled with an internal solution that contained: 130 mM Cs-methanesulfonate, 5 mM NaCl, 10 mM EGTA, 10 mM HEPES, 10 mM phosphocreatine, and 2 mM Mg-ATP, pH 7.3 with CsOH, 290–300 mOsm. The cells were held at a holding potential of −70 mV. For mini recordings, slices were also perfused with 500 nM TTX. The mEPSCs were detected using Axograph X software and the mEPSCs were detected using a template based detection algorithm package. Synaptic responses were evoked every 15 sec using a clustered electrode (FHC) and the stimulus electrode was placed in the stratum radiatum near the CA3/CA1. To measure paired pulse ratios (PPR), pairs of 20 Hz and 40 Hz were delivered and averages of at least 6 sweeps were analyzed. PPR was calculated as a ratio of EPSC2/EPSC1.

Electron microscopy—Animals (postnatal day 21, $mSYD1A^{KO}$ and wild-type littermates) were transcardially perfused with fixative (2 % paraformaldehyde, 2 % glutaraldehyde in 100 mM phosphate buffer pH 7.4) and brains were postfixed for 1 h. Tissues were sectioned coronally at 60 μm thickness in PBS on a vibratome. Sections from the same frontcaudal brain region (Bregma −1.9) were analyzed for each genotype. Sections were washed in 0.1 M cacodylate buffer, pH 7.4, postfixed in 0.1 M reduced osmium (1.5 % $K_4Fe(CN)_6$, 1 % OsO4 in water) and embedded in Epon resin. The *stratum radiatum* of area CA1 was identified using the pyramidal cell layer and the alveus as landmarks. Images were acquired on a Transmission Electron Microscope (Fei Morgagni, 268D). Quantification of the number and distribution of vesicles was performed using XtraCount software (developed by C. Olendrowitz, Göttingen, Germany). All image acquisition and analysis was done blinded with respect to the genotype of the animals. Independent datasets were collected from 4 KO and 4 wild-type animals. For each animal, at least 35 9.3 μm^2 fields were acquired and at least 83 synapses analyzed. The total number of synapses quantitatively analyzed was 404 for wild-type and 366 for KO material.

Light microscopy—Images were acquired on a LSM5 confocal microscope (Zeiss, Germany) and assembled using Adobe Photoshop and Illustrator software. For the analysis of dendritic arborization, neurons were traced and analyzed with Neurolucida (MBF Bioscience). The identification of axons vs. dendrites is based on the unique characteristics of cerebellar granule cells, which exhibit 3–5 short dendritic processes and a thinner, much more elongated axon.

Co-localization analysis of proteins in COS cells was performed by the Pearson's coefficient method computed on fluorograms, using the JaCOP plugin in ImageJ (Bolte and Cordelieres, 2006).

Quantification of pre- and postsynaptic proteins in granule cells was performed by a wavelet-based segmentation method, using the Multidimensional Image Analysis module (Racine et al., 2006; Izeddin et al., 2012), run in Metamorph software (Molecular Devices, USA). Puncta on different channels were segmented and counted by thresholding the third wavelet map with a value ranging from 15 to 35 times the noise standard deviation.

Some images for figures were processed by deconvolution using a theoretical PSF, a signal/noise ratio of 10 for each channel and 30 iterations of the deconvolution algorithm (Huygens remote manager v2.1.2).

Acknowledgments

We thank Yves Barde, Casper Hoogenraad, Eunjoon Kim, Thi-Minh Nguyen, Olivier Pertz, Susanne Schoch, Dietmar Schreiner, Tim Sharpe, Stephan Sigrist, Matthijs Verhage, Mingjie Zhang for valuable reagents and advice. We thank Ursula Sauder and the Zentrum für Mikroskopie for excellent support with the electron microscopy and Daniela Klewe-Nebenius and the Transgenic Mouse Core Facility for help in generating the $mSYD1A^{KO}$ mice. This work was supported by a fellowship from the Werner-Siemens Foundation to C.W., an award from the Boehringer Ingelheim Fund to J.E.S., funds to P.S. from the Swiss National Science Foundation, the National Institute on Drug Abuse, and the Kanton Basel-Stadt.

References

Ackley BD, Harrington RJ, Hudson ML, Williams L, Kenyon CJ, Chisholm AD, Jin Y. The two isoforms of the Caenorhabditis elegans leukocytecommon antigen related receptor tyrosine phosphatase PTP-3 function independently in axon guidance and synapse formation. Journal of Neuroscience. 2005; 25:7517–7528. [PubMed: 16107639]

Arikkath J, Reichardt LF. Cadherins and catenins at synapses: roles in synaptogenesis and synaptic plasticity. Trends in Neurosciences. 2008; 31:487–494. [PubMed: 18684518]

Ball RW, Warren-Paquin M, Tsurudome K, Liao EH, Elazzouzi F, Cavanagh C, An BS, Wang TT, White JH, Haghighi AP. Retrograde BMP Signaling Controls Synaptic Growth at the NMJ by Regulating Trio Expression in Motor Neurons. Neuron. 2010; 66:536–549. [PubMed: 20510858]

Biederer T, Stagi M. Signaling by synaptogenic molecules. Curr. Opin. Neurobiol. 2008; 18:261–269. [PubMed: 18725297]

Bolte S, Cordelieres FP. A guided tour into subcellular colocalization analysis in light microscopy. Journal of Microscopy. 2006; 224:213–232. [PubMed: 17210054]

Cheadle L, Biederer T. The novel synaptogenic protein Farp1 links postsynaptic cytoskeletal dynamics and transsynaptic organization. Journal of Cell Biology. 2012; 199:985–1001. [PubMed: 23209303]

Dai Y, Taru H, Deken SL, Grill B, Ackley B, Nonet ML, Jin Y. SYD-2 Liprin-a organizes presynaptic active zone formation through ELKS. Nature Neuroscience. 2006; 9:1479–1487.

de Vries KJ, Geijtenbeek A, Brian EC, de Graan PN, Ghijsen WE, Verhage M. Dynamics of munc18-1 phosphorylation/dephosphorylation in rat brain nerve terminals. European Journal of Neuroscience. 2000; 12:385–390. [PubMed: 10651895]

Dean C, Scholl FG, Choih J, DeMaria S, Berger J, Isacoff E, Scheiffele P. Neurexin mediates the assembly of presynaptic terminals. Nature Neuroscience. 2003; 6:708–716.

Dyson HJ, Wright PE. Intrinsically unstructured proteins and their functions. Nature Reviews Molecular Cell Biology. 2005; 6:197–208.

Frank CA, Pielage J, Davis GW. A presynaptic homeostatic signaling system composed of the Eph receptor, Ephexin, Cdc42 and Ca2.1 Calcium Channels. Neuron. 2009; 61:556–569. [PubMed: 19249276]

Galea CA, Pagala VR, Obenauer JC, Park CG, Slaughter CA, Kriwacki RW. Proteomic studies of the intrinsically unstructured mammalian proteome. J. Proteome Res. 2006; 5:2839–2848. [PubMed: 17022655]

Gascon S, Paez-Gomez JA, Diaz-Guerra M, Scheiffele P, Scholl FG. Dual-promoter lentiviral vectors for constitutive and regulated gene expression in neurons. Journal of Neuroscience Methods. 2008; 168:104–112. [PubMed: 17983662]

Graham DL, Eccleston JF, Lowe PN. The conserved Arginine in Rho-GTPas-activating protein is essential for efficient catalysis but not for complex formation with RhoGDP and Aluminium Fluoride. Biochemistry. 1999; 38:985–991. [PubMed: 9893994]

Gundelfinger ED, Fejtova A. Molecular organization and plasticity of the cytomatrix at the active zone. Current Opinion in Neurobiology. 2012; 22:423–430. [PubMed: 22030346]

Hackel M, Konno T, Hinz H. A new alternative method to quantify residual structure in 'unfolded' proteins. Biochim. Biophys. Acta. 2000; 1479:155–165. [PubMed: 11004537]

Hallam SJ, Goncharov A, McEwen J, Baran R, Jin Y. SYD-1, a presynaptic protein with PDZ, C2 and rhoGAP-like domains, specifies axon identity in C. elegans. Nature Neuroscience. 2002; 5:1137–1146.

Han YY, Kaeser PS, Südhof TC, Schneggenburger R. RIM Determines Ca2+ Channel Density and Vesicle Docking at the Presynaptic Active Zone. Neuron. 2011; 69:304–316. [PubMed: 21262468]

Ishida T, Kinoshita K. Prediction of disordered regions in proteins based on the meta approach. Bioinformatics. 2008; 24:1344–1348. [PubMed: 18426805]

Itoh RE, Kurokawa K, Ohba Y, Yoshizaki H, Mochizuki N, Matsuda M. Activation of rac and cdc42 video imaged by fluorescent resonance energy transfer-based single-molecule probes in the membrane of living cells. Molecular and Cellular Biology. 2002; 22:6582–6591. [PubMed: 12192056]

Izeddin I, Boulanger J, Racine V, Specht CG, Kechkar A, Nair D, Triller A, Choquet D, Dahan M, Sibarita JB. Wavelet analysis for single molecule localization microscopy. Opt. Express. 2012; 20:2081–2095. [PubMed: 22330449]

Jin Y, Garner CC. Molecular mechanisms of presynaptic differentiation. Annu. Rev. Cell Dev. Biol. 2008; 24:237–262. [PubMed: 18588488]

Jockusch WJ, Speidel D, Sigler A, Sorensen JB, Varoqueaux F, Rhee JS, Brose N. CAPS-1 and CAPS-2 are essential synaptic vesicle priming proteins. Cell. 2007; 131:796–808. [PubMed: 18022372]

Johnson EL 3rd, Fetter RD, Davis GW. Negative regulation of active zone assembly by a newly identified SR protein kinase. PLoS Biology. 2009; 7:e1000193. [PubMed: 19771148]

Ko J, Na M, Kim S, Lee JR, Kim E. Interaction of the ERC family of RIM-binding proteins with the liprin-alpha family of multidomain proteins. Journal of Biological Chemistry. 2003; 278:42377–42385. [PubMed: 12923177]

Kwon S-K, Woo J, Kim S-Y, Kim H, Kim E. Trans-synaptic adhesions between Netrin-G Ligand-3 (NGL-3) and receptor tyrosine phosphatases LAR, protein-tyrosine phosphatase d (PTPd), and PTPs via specific domains regulate excitatory synapse formation. Journal of Biological Chemistry. 2010; 285:13966–13978. [PubMed: 20139422]

Marra V, Burden JJ, Thorpe JR, Smith IT, Smith SL, Hausser M, Branco T, Staras K. A preferentially segregated recycling vesicle pool of limited size supports neurotransmission in native central synapses. Neuron. 2012; 76:579–589. [PubMed: 23141069]

Miskiewicz K, Jose LE, Bento-Abreu A, Fislage M, Taes I, Kasprowicz J, Swerts J, Sigrist S, Versees W, Robberecht W, Verstreken P. ELP3 controls active zone morphology by acetylating the ELKS family member Bruchpilot. Neuron. 2011; 72:776–788. [PubMed: 22153374]

Owald D, Fouquet W, Schmidt M, Wichmann C, Mertel S, Depner H, Christiansen F, Zube C, Quentin C, Körner J, et al. A Syd-1 homologue regulates pre- and postsynaptic maturation in Drosophila. Journal of Cell Biology. 2010; 188:565–579. [PubMed: 20176924]

Owald D, Khorramshahi O, Gupta VK, Banovic D, Depner H, Fouquet W, Wichmann C, Mertel S, Eimer S, Reynolds E, et al. Cooperation of Syd-1 with Neurexin synchronizes pre- with postsynaptic assembly. Nature Neuroscience. 2012; 15:1219–1226.

Patel MR, Lehrman EK, Poon VY, Crump JG, Zhen M, Bargmann CI, Shen K. Hierarchical assembly of presynaptic components in defined C. elegans synapses. Nature Neuroscience. 2006; 9:1488–1498.

Pertz O, Hodgson L, Klemke RL, Hahn KM. Spatiotemporal dynamics of RhoA activity in migrating cells. Nature. 2006; 440:1069–1072. [PubMed: 16547516]

Racine V, Sachse M, Salamero J, Fraisier V, Trubuil A, Sibarita J-B. Visualization and quantification of vesicle trafficking on a three-dimensional cytoskeleton network in living cells. Journal of Microscopy. 2006; 225:214–228. [PubMed: 17371444]

Schikorski T, Stevens CF. Morphological correlates of functionally defined synaptic vesicle populations. Nature Neuroscience. 2001; 4:391–395.

Shen K, Scheiffele P. Genetics and cell biology of building specific synaptic connectivity. Annual Review of Neuroscience. 2010; 33:473–507.

Sigrist SJ, Schmitz D. Structural and functional plasticity of the cytoplasmic active zone. Curr Opin Neurobiol. 2011; 21:144–150. [PubMed: 20832284]

Siksou L, Varoqueaux F, Pascual O, Triller A, Brose N, Marty S. A common molecular basis for membrane docking and functional priming of synaptic vesicles. European Journal of Neuroscience. 2009; 30:49–56. [PubMed: 19558619]

Skarnes WC, Rosen B, West AP, Koutsourakis M, Bushell W, Iyer V, Mujica AO, Thomas M, Harrow J, Cox T, et al. A conditional knockout resource for the genome-wide study of mouse gene function. Nature. 2011; 474:337–342. [PubMed: 21677750]

Spangler SA, Jaarsma D, De Graaff E, Wulf PS, Akhmanova A, Hoogenraad CC. Differential expression of liprin-alpha family proteins in the brain suggests functional diversification. Journal of Comparative Neurology. 2011; 519:3040–3060. [PubMed: 21618222]

Stavoe AK, Colon-Ramos DA. Netrin instructs synaptic vesicle clustering through Rac GTPase, MIG-10, and the actin cytoskeleton. Journal of Cell Biology. 2012; 197:75–88. [PubMed: 22451697]

Südhof TC. The presynaptic active zone. Neuron. 2012; 75:11–25. [PubMed: 22794257]

Sun Y, Bamji SX. beta-Pix modulates actin-mediated recruitment of synaptic vesicles to synapses. Journal of Neuroscience. 2011; 31:17123–17133. [PubMed: 22114281]

Takahashi H, Arstikaitis P, Prasad T, Bartlett TE, Wang YT, Murphy TH, Craig AM. Postsynaptic TrkC and Presynaptic PTPsigma function as a bidirectional excitatory synaptic organizing complex. Neuron. 2011; 69:287–303. [PubMed: 21262467]

Taniguchi H, Gollan L, Scholl FG, Mahadomrongkul V, Dobler E, Limthong N, Peck M, Aoki C, Scheiffele P. Silencing of neuroligin function by postsynaptic neurexins. Journal of Neuroscience. 2007; 27:2815–2824. [PubMed: 17360903]

Tompa P. Intrinsically disordered proteins: a 10-year recap. Trends in Biochemical Sciences. 2012; 37:509–516. [PubMed: 22989858]

Toonen RF, Wierda K, Sons MS, de Wit H, Cornelisse LN, Brussaard A, Plomp JJ, Verhage M. Munc18-1 expression levels control synapse recovery by regulating readily releasable pool size. Proceedings of the National Academy of Sciences. 2006; 103:18332–18337.

Verhage M, Sorensen JB. Vesicle docking in regulated exocytosis. Traffic. 2008; 9:1414–1424. [PubMed: 18445120]

Wei Z, Zheng S, Spangler SA, Yu C, Hoogenraad CC, Zhang M. Liprin-mediated large signaling complex organization revealed by the Liprin-a/CASK and Liprin-a/Liprin-b complex structures. Molecular Cell. 2011; 43:586–598. [PubMed: 21855798]

Weimer RM, Richmond JE, Davis WS, Hadwiger G, Nonet ML, Jorgensen EM. Defects in synaptic vesicle docking in unc-18 mutants. Nature Neuroscience. 2003; 6:1023–1030.

Woo J, Kwon SK, Choi S, Kim S, Lee JR, Dunah AW, Sheng M, Kim E. Trans-synaptic adhesion between NGL-3 and LAR regulates the formation of excitatory synapses. Nature Neuroscience. 2009; 12:428–437.

Yoshida T, Yasumura M, Uemura T, Lee S-J, Ra M, Taguchi R, Iwakura Y, Mishina M. IL-1 receptor accessory protein-like 1 associated with mental retardation an autism mediates synapse formation by trans-synaptic interaction with protein tyrosine phosphatese delta. Journal of Neuroscience. 2011; 31:13485–13499. [PubMed: 21940441]

Zhai RG, Bellen HJ. The architecture of the active zone in the presynaptic nerve terminal. Physiology. 2004; 19:262–270. [PubMed: 15381754]

Ziv NE, Garner CC. Cellular and molecular mechanisms of presynaptic assembly. Nature Reviews Neuroscience. 2004; 5:385–399.

Zürner M, Mittelstaedt T, Dieck ST, Becker A, Schoch S. Analysis of the spatiotemporal expression and subcellular localization of Liprin-alpha proteins. Journal of Comparative Neurology. 2011; 519:3019–3039. [PubMed: 21618221]

Zürner M, Schoch S. The mouse and human Liprin-alpha family of scaffolding proteins: genomic organization, expression profiling and regulation by alternative splicing. Genomics. 2009; 93:243–253. [PubMed: 19013515]

Supplementary Material

Refer to Web version on PubMed Central for supplementary material.

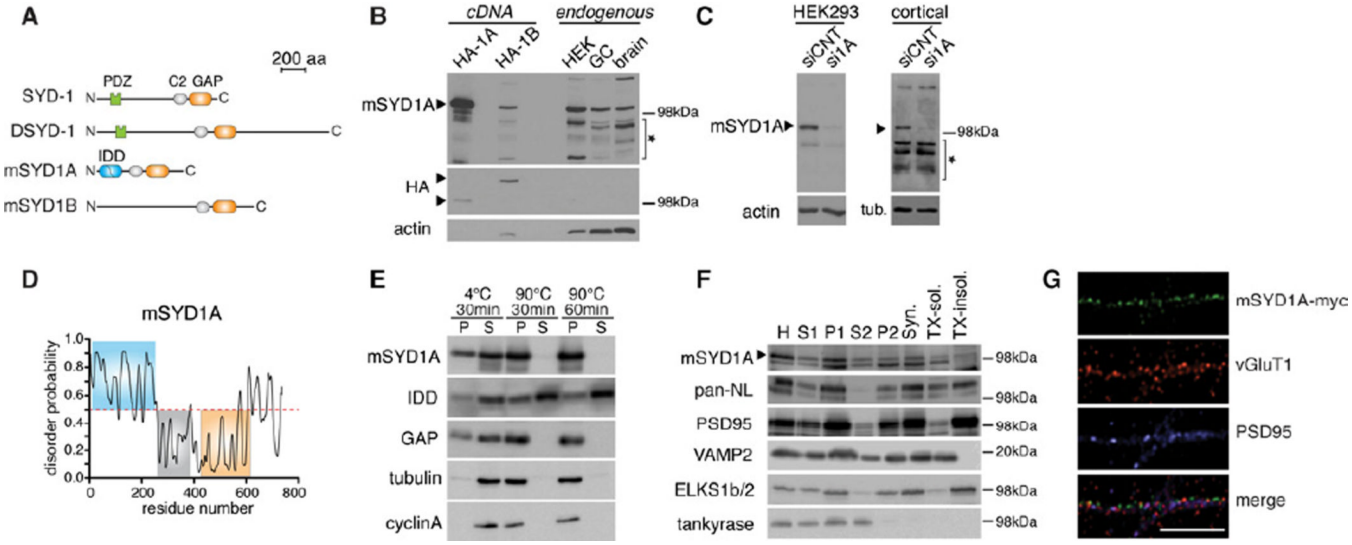

Figure 1. Identification and characterization of mSYD1A

(**A**) Predicted domain structure of *C.elegans* SYD-1, *Drosophila* DSYD-1, mouse mSYD1A and mouse mSYD1B. See Figure S1A,B for further information on mSYD1A sequence analysis.

(**B**) Western blot with anti-mSYD1A antibodies on HA-tagged mSYD1A and mSYD1B overexpressed in HEK293T cells (HA-1A, HA-1B), untransfected HEK293T cells, cerebellar granule neurons (GC) and P5 mouse brain lysate (brain). The star marks unspecific bands. Note that higher amounts of cell lysates were loaded for detection of endogenous proteins to enable direct size comparison with the protein expressed from cDNA.

(**C**) The 100 kDa mSYD1A-immuno-reactive band is lost after treatment of cultured HEK293T cells and cortical neurons with *syd1a* specific siRNAs (si1A) but not nontargeting control siRNAs (siCNT). See Figure S1C for developmental expression profile of mSYD1A protein.

(**D**) The N-terminal region of mSYD1A is predicted to be instrinsically disordered (http://prdos.hgc.jp/cgi-bin/top.cgi). Residues with score above a 0.5 are predicted to be disordered.

(**E**) The intrinsically disordered N-terminal domain of mSYD1A (IDD) is heat stable. Cytoplasmic extracts from HEK293T cells expressing mSYD1A, IDD or GAP domain, were incubated at indicated times and temperatures. Upon incubation soluble (S) and insoluble (P) proteins were separated by centrifugation. Tubulin and cyclin A were used as endogenous globular control proteins.

(**F**) Synaptosome fractionation of adult mouse brain. 10 μg of proteins were loaded for each fraction. H: homogenate; Syn.: synaptosomes; TX-sol.: Triton X-100 soluble synaptic proteins; TX-insol.: Triton X-100 insoluble synaptic protein complexes.

(**G**) In the axon of cultured cerebellar granule cells overexpressed mSYD1A with a Cterminal myc-epitope shows a punctate distribution partially overlapping with vGluT1/PSD95 puncta (scalebar = 10 μm).

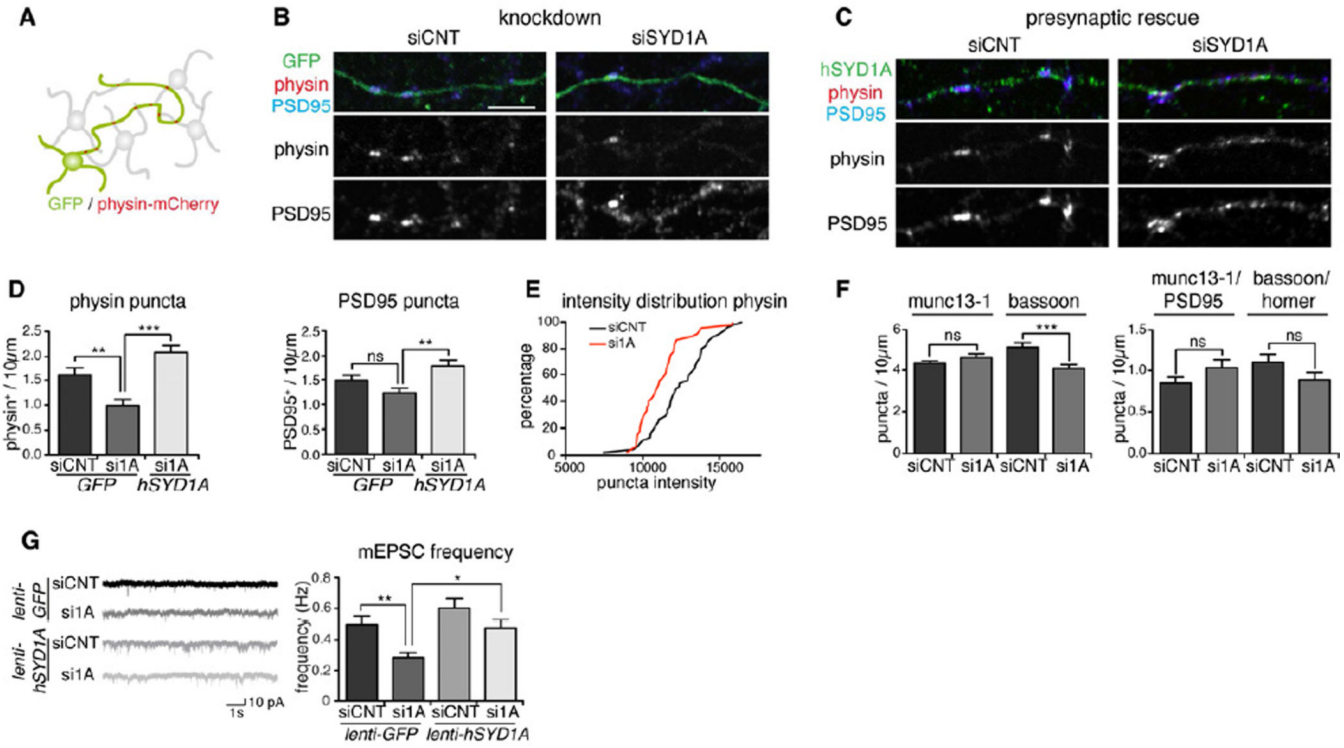

Figure 2. Knockdown of mSYD1A decreases synaptic vesicle clustering

(**A**) Global knockdown of mSYD1A is combined with selective marking of a subset of cerebellar granule cells using EGFP and synaptophysin-mCherry. For selective presynaptic rescue of mSYD1A, siRNA-resistant hSYD1A is expressed in a small subset of cells. See Figure S2G,H for validation of the synaptophysin-mCherry marker.

(**B**) Accumulation of synaptophysin-mCherry (physin) and endogenous PSD95 along transfected neurons in control (siCNT) and mSYD1A knockdown (siSYD1A) neurons (note that cell penetrating siRNAs result in mSYD1A knock-down in nearly all cells in culture). See Figure S2A–D for further control experiments and morphological analysis of mSYD1A knock-down cells. Scalebar = 10 µm.

(**C**) Rescue of the knockdown was achieved by transfection of a small sub-population of cells with siSYD1A-resistant human SYD1A (hSYD1A).

(**D**) Quantitative analysis of synaptic markers. The number of physin^{+} or PSD95^{+} puncta and physin/PSD95 double positive puncta per 10 µm axon length were counted (n=45 cells; *: p<0.05; ***: p<0.0001; ANOVA and Tukey's multiple comparison test; mean ± s.e.m.).

(**E**) Cumulative distribution of staining intensities for synaptophysin-mCherry-positive puncta in siCNT and siSYD1A-treated neurons.

(**F**) Number of munc13-1^{+}, bassoon^{+} and munc13-1/PSD95, bassoon/homer double positive puncta per 10 µm axon length (n=45 cells; ns: not significant; ***: p=0.0001; two-tailed t-test; mean ± s.e.m.).

(**G**) Recordings of mEPSC events from cerebellar granule cells infected with a lentivirus driving expression of EGFP or EGFP and hSYD1A (rescue) in close to 100% of the cells and treated with siCNT or siSYD1A (n=30 cells; *: p<0.05; **: p<0.001; ***: p<0.0001; ns: not significant; non-parametric ANOVA and Dunn's multiple comparison test; mean ± s.e.m.). See Figure S2E,F for protein expression level in the rescue experiments and mEPSC amplitude measurements.

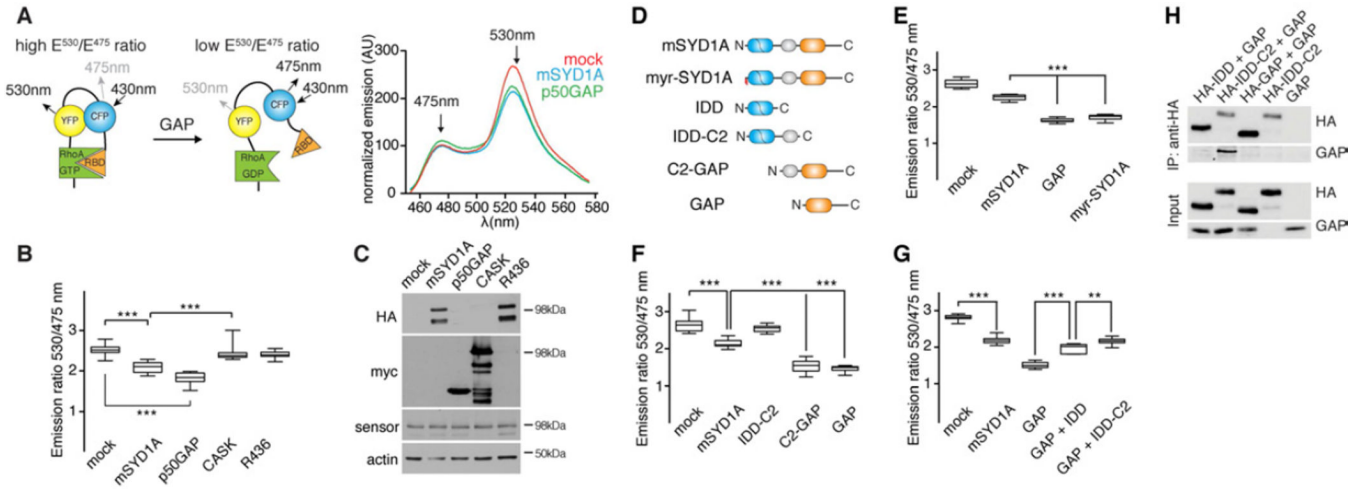

Figure 3. mSYD1A exhibits GAP activity towards RhoA

(**A**) FRET sensor for the measurement of GAP activity towards RhoA. HEK293T cells were co-transfected with expression constructs for RhoA sensor and mSYD1A or p50rhoGAP. The emission spectra for excitation at 433 nm were normalized by subtraction of signals obtained with control cells lacking sensor expression. RBD: Rhobinding domain of the effector rhotekin.

(**B**) Emission ratios (Intensity 530nm/Intensity 475nm) from FRET sensor assays (n=12 replicates; **: p<0.001; ***: p<0.0001; ns: not significant; ANOVA and Tukey's multiple comparison test; line at median, whiskers: min to max). See Figure S3A,B for explanation of Rho-GAP domain point mutations in mSYD1A.

(**C**) Expression of the RhoA sensor and co-expressed proteins (anti-HA and anti-Myc antibodies) were verified by western blotting after completing the FRET measurements in the same extracts.

(**D**) mSYD1A deletion constructs. N-terminal lipid modification (myristoylation and palmitoylation) is marked in red. See Figure S3C for protein expression level of the various deletion constructs.

(**E-G**) Emission ratios (Intensity 530 nm/Intensity 475 nm) observed for mSYD1A constructs (n=12 replicates; ***: p<0.0001; ANOVA and Tukey's multiple comparison test; line at median, whiskers: min to max). For GAP+IDD and GAP+IDD-C2, two mSYD1A deletion constructs were co-expressed in the same cell.

(**H**) Co-immunoprecipiation of proteins co-transfected in HEK293T cells. Anti-HA immunoprecipitates (IP) were probed with anti-HA and anti-Myc antibodies.

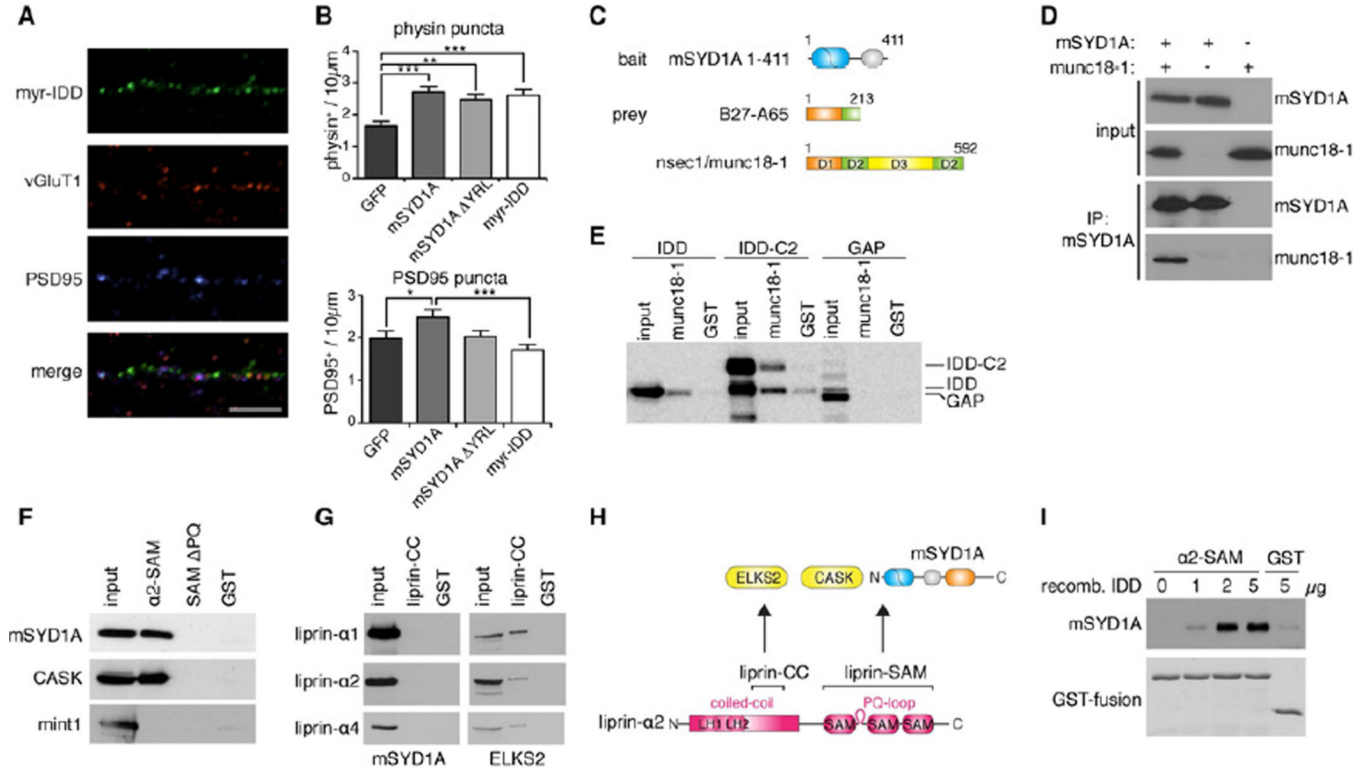

Figure 4. Identification of the mSYD1A disordered domain as a key determinant for presynaptic differentiation

(**A**) Overexpressed Myr-IDD(mSYD1A) in cerebellar granule cells partially overlaps with vGluT1/PSD95 puncta (scalebar = 10 µm). See Figure S4A for data on overexpression in mSYD1A knock-out neurons.

(**B**) Overexpression of mSYD1A truncation constructs in neurons (transient transfection of a subset of cells as in Figure 2A). Number of physin or PSD95 puncta per 10 µm axon length in cerebellar granule cells overexpressing GFP or mSYD1A constructs (n=30 cells; *: $p<0.05$; **: $p<0.001$; ***: $p<0.0001$, ANOVA and Tukey's multiple comparison test; mean ± s.e.m.).

(**C**) A yeast-2-hybrid screen with an mSYD1A truncation construct, containing amino acids 1 – 411, as bait, led to the identification of nsecI/munc18-1 as a potential mSYD1A binding partner. Clone B27-A65 encoding amino acids 1 – 213 of nsec-1/munc18-1 was recovered.

(**D**) Munc18-1, overexpressed in HEK293T cells, co-immunoprecipitates with overexpressed mSYD1A.

(**E**) His-tagged munc18-1, coupled to beads, was incubated with HEK293T cell lysate overexpressing different deletion constructs of mSYD1A. Note that the IDD-C2 domain protein is sensitive to proteolysis resulting in partial removal of the C2 domain (lower band).

(**F**) Beads containing liprin-α2 SAM domains with (α2-SAM) or without the PQ-loop (SAM ΔPQ) were incubated with HEK293T cell lysates containing overexpressed mSYD1A, CASK or mint1. Recombinant GST was used as negative control (GST). Equivalent fractions of input and bound proteins were analyzed by Western blotting. See Figure S4B for the recombinant proteins used in the pull-down assay.

(**G**) Beads containing recombinant liprin-a1, α2, and α4 coiled-coil domain fragments (liprin-CC) were incubated with HEK293T cell lysates containing overexpressed mSYD1A or ELKS2.

(**H**) Domain organization of liprin-αL fragments used in pull-down assays, and protein interaction sites. LH1 and LH2 denote highly conserved liprin homology regions. Liprin-α

contains an alternative splice insertion between the first and the second SAM domain (PQ-loop), which is absent from the most abundant liprin-α1 isoform.
(**I**) Binding assay with purified recombinant liprin-α2 SAMand increasing amounts of purified recombinant ID-domain of mSYD1A (IDD). See Figure S4C for data on pulldown experiments performed from cell extracts.

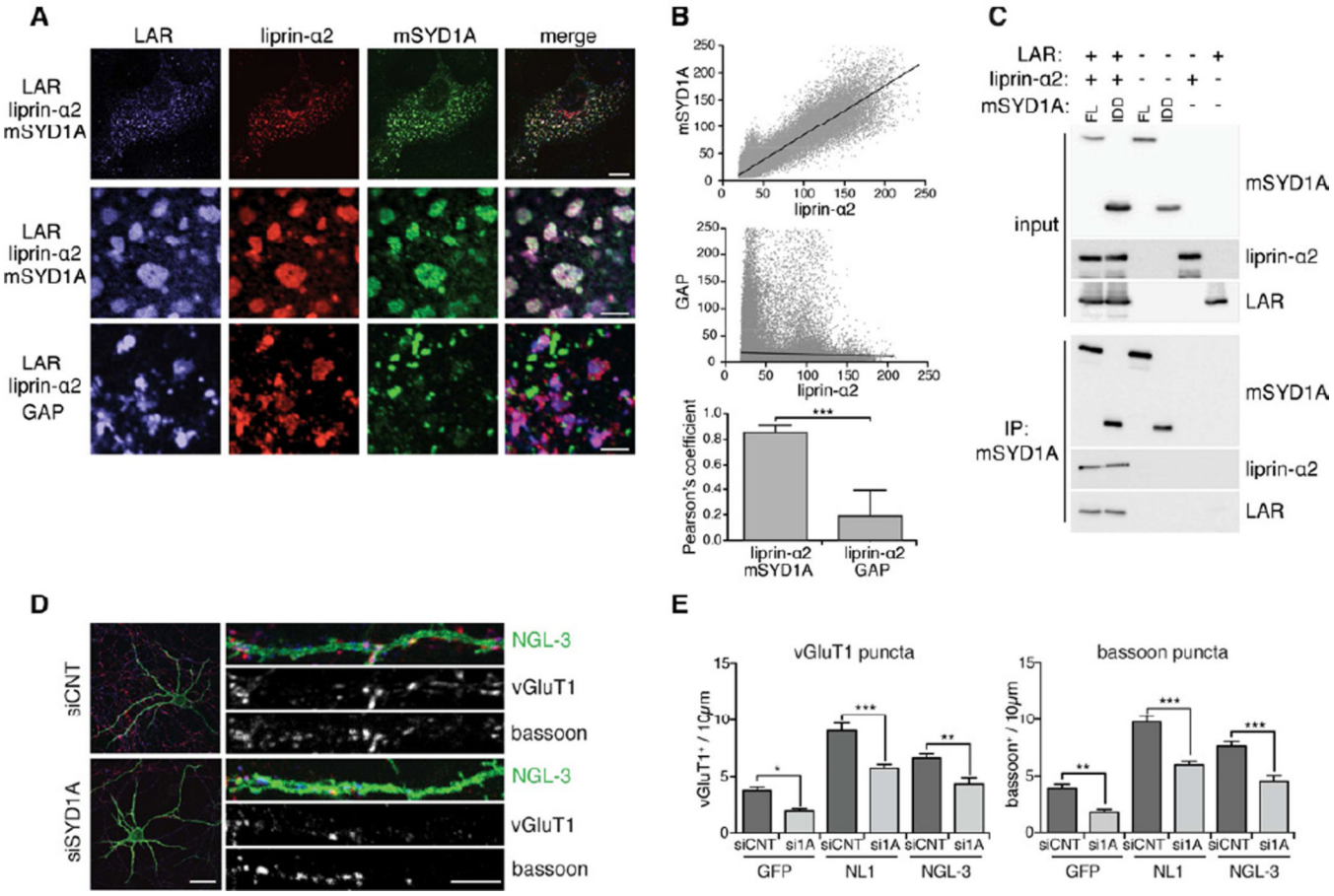

Figure 5. mSYD1A is recruited into LAR/liprin-α2 complexes

(**A**) COS7 cells, triple transfected with expression constructs for liprin-α2, LAR, and/or mSYD1A. Upper rows show entire cells (scalebar = 10 μm), lower rows show enlargement of sub-membrane clusters (scalebar = 5 μm). See Figure S5A–C for colocalization analysis on single and double-transfected cells.

(**B**) Quantitative colocalization analysis of LAR, liprin-α2, mSYD1A co-expressing cells. Scatter plots display pixel values of liprin-α2 and mSYD1A, or liprin-α2 and mSYD1A GAP immune-reactivities. The mean Pearson's coefficient provides a quantitative measure for the distribution of the observed puncta (n=10 cells; two-tailed t-test, ***: $p<0.0001$; mean ± s.d.).

(**C**) Co-immunoprecipitation of liprin-α2 and LAR with mSYD1A full-length (FL) and a construct containing only the ID-domain (IDD) of mSYD1A.

(**D**) Cerebellar granule cells treated with control (siCNT) or mSYD1A (siSYD1A) siRNAs resulting in knock-down in all cells in culture. A small subset of cells was transfected with expression vectors for NGL-3 (green). Presynaptic terminals are visualized by immunostaining for endogenous vGluT1 (red) and bassoon (blue) (scalebar overview = 20 μm, scalebar segment = 5 μm). See Figure S5D for analysis of NGL-3 expression level in mSYD1A knock-down cells.

(**E**) Quantification of the density of $vGluT1^+$ and $bassoon^+$ puncta along the dendrites of GFP, neuroligin-1 (NL1) or NGL-3 expressing neurons (n = 25 cells; *: $p<0.05$; **: $p<0.001$; ***: $p<0.0001$; ANOVA and Tukey's multiple comparison test, mean ± s.e.m.).

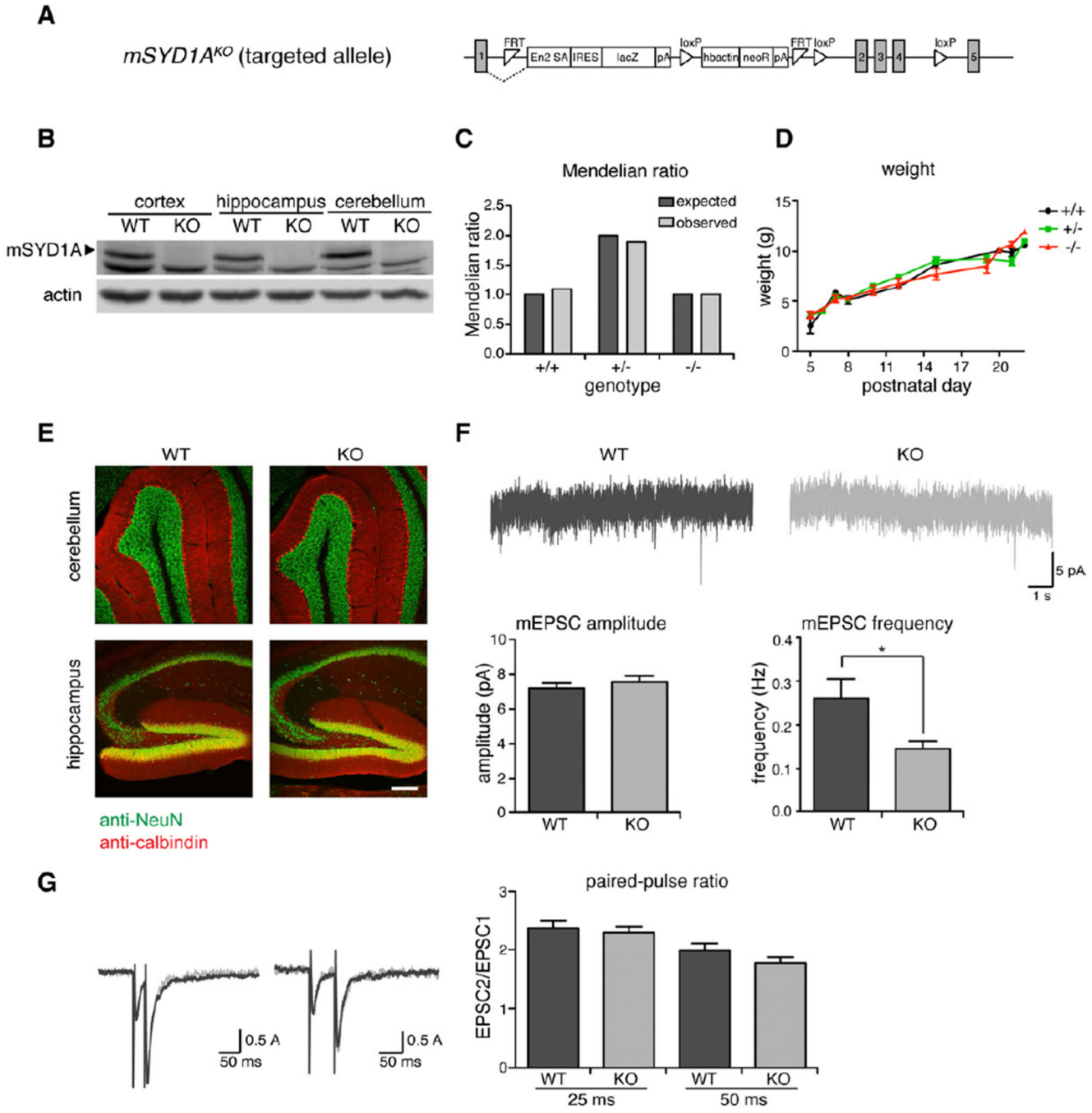

Figure 6. Reduced synaptic transmission in *mSYD1A*^{KO} hippocampus

(**A**) Targeted EUCOMM *mSYD1A*^{KO} allele: A genetrap insertion following exon 1 introduces a strong splice acceptor site (En2 SA) linked to lacZ open-reading frame. In addition, exons 2–4 are flanked by loxP sites.

(**B**) mSYD1A protein expression is completely lost in *mSYD1A*^{KO} mice.

(**C**) *mSYD1A*^{KO} mice are born at Mendelian frequencies.

(**D**) Weight gain in *mSYD1A*^{KO} mice is comparable to WT mice during the first 4 weeks of age.

(**E**)$mSYD1A^{KO}$ mice do not show any alterations is gross morphology of cerebellum and hippocampus compared to WT mice.
(**F**) Recordings of mEPSC frequency and amplitude from CA1 neurons in acute hippocampal slices of $mSYD1A^{KO}$ mice and WT littermate control mice at age P13–15 ($n \geq 18$ cells from 4 animals per genotype; *: $p<0.05$; two-tailed t-test; mean ± s.e.m.).
(**G**) Measurements of paired-pulse ratio at 25 ms and 50 ms intervals of $mSYD1A^{KO}$mice and WT littermate controls at age P11–16 ($n \geq 18$ cells per genotype; two-tailed t-test; mean ± s.e.m.).

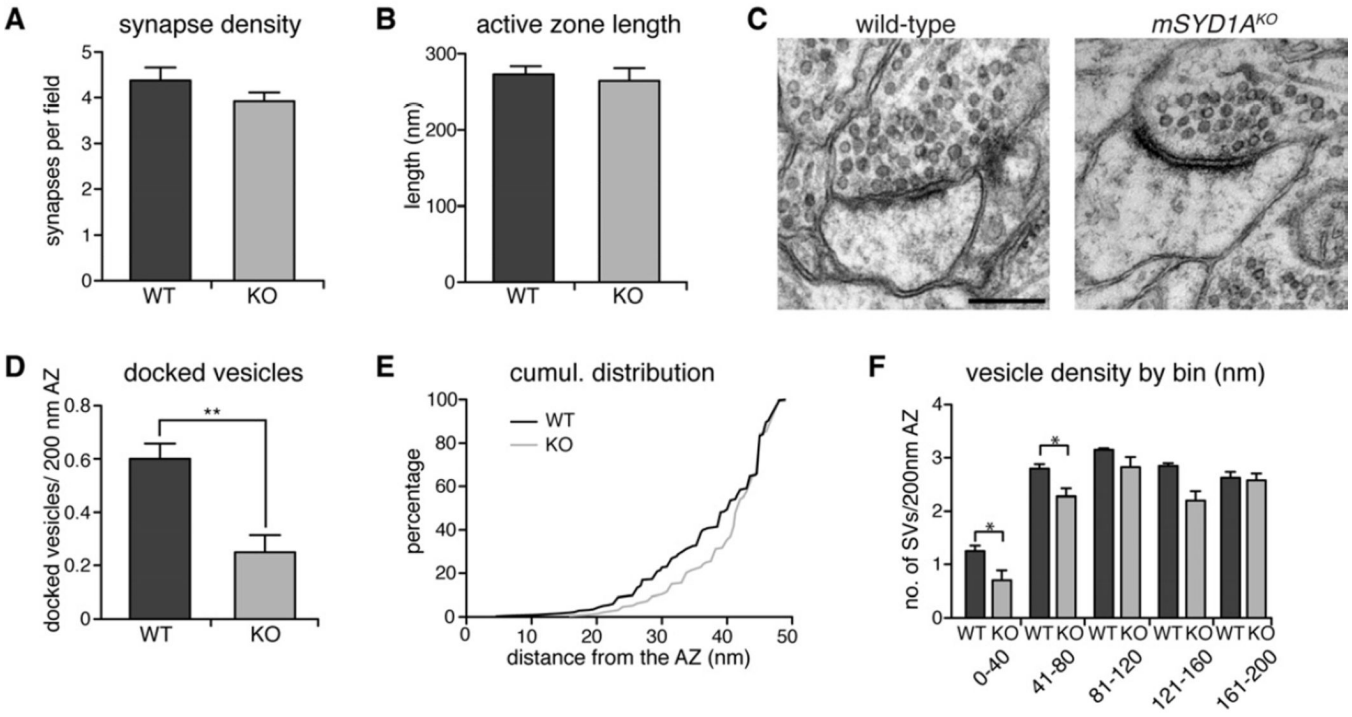

Figure 7. Impaired synaptic vesicle docking in *mSYD1A^{KO}* mice

(**A,B**) Average active zone length and synapse density are not changed between *mSYD1A^{KO}* and WT mice (147 WT and 157 KO fields of 9.3 μm^2, AZ length analyzed for 404 WT and 366 KO synapses, from 4 WT and 4 KO mice; two-tailed t-test; mean ± s.e.m.).

(**C**) Ultrastructure of synapses from *mSYD1A^{KO}* and WT control littermates in the CA1 region of the hippocampus at P21 (scalebar = 200 nm).

(**D**) The number of docked vesicles / 200 nm active zone is significantly reduced in *mSYD1A^{KO}* compared to WT control mice. Docked vesicles were defined as vesicles with center within 30 nm distance of the active zone, a distance where the vesicle membrane directly abuts the presynaptic membrane (404 WT and 366 KO synapses analyzed from 4 WT and 4 KO mice, **: $p<0.001$; two-tailed t-test; mean ± s.e.m.).

(**E**) Cumulative frequency distribution of all synaptic vesicles within 50 nm distance to the active zone (≥ 543 vesicles per genotype from 4 WT and 4 KO mice; KS test: $p = 0.001$).

(**F**) Average number of vesicles located in 40 nm bins with increasing distance from the active zone normalized to 200 nm active zone length (404 WT and 366 KO synapses analyzed from 4 WT and 4 KO mice, *: $p<0.05$; two-tailed t-test; mean ± s.e.m.).